Journal of Inclusion Phenomena and Macrocyclic Chemistry **41:** 155–162, 2001.

Selective Binding of Open Frameworks Assembled from Nickel(II) Macrocyclic Complexes with Organic and Inorganic Guests *

HYE JIN CHOI, TAEK SOON LEE and MYUNGHYUN PAIK SUH**
School of Chemistry and Center for Molecular Catalysis, Seoul National University, Seoul 151-747, Republic of Korea

(Received: 15 July 2001; in final form: 31 August 2001)

Key words: guest binding, nickel(II) macrocycle, open framework, self-assembly, supramolecular chemistry

Abstract

Inclusion studies for metal-organic open-frameworks, $[Ni(C_{10}H_{24}N_4)(H_2O)_2]_3[BTC]_2{\cdot}24H_2O$ (**1**) and $[Ni(C_{10}H_{26}N_6)]_3[BTC]_2{\cdot}18H_2O$ (**2**) (BTC^{3-} = 1,3,5-benzenetricarboxylate) with various organic and inorganic guest molecules have been carried out. **1** is the previously reported molecular floral lace with 1-D channels, where positively charged macrocyclic layers and negatively charged BTC^{3-} layers are alternately packed by hydrogen bonding interactions. **2** is assembled in this study from nickel(II) hexaazamacrocyclic complex containing methyl pendant arms and BTC^{3-}. The X-ray structure of **2** shows that the nickel(II) complex and BTC^{3-} form a 2-D coordination polymer. The XRPD patterns of **2** indicate that framework of **2** is slightly deformed upon removal of water guest molecules but restored upon rebinding of water. The host solid **1** binds MeOH in toluene, and 1,3,5-trihydroxybenzene (THB) and 4-hydroxyacetophenone (HAP) in EtOH/toluene (v/v = 1/4) solutions. The binding constants (K_f) of **1** for MeOH, THB, and HAP are 66.4 M^{-1}, 259 M^{-1}, and 13.9 M^{-1}, respectively. In the range of high concentration of the guest, however, the host shows various binding curves depending upon the types of guest. It binds PhOH in toluene, showing a sigmoid curve. It also binds transition metal complexes such as $[Cu(NH_3)_4](ClO_4)_2$, $[Cu(ethylenediamine)_2](ClO_4)_2$, $[Cu(histamine)_2](ClO_4)_2$, and [Cu(*N*,*N*′-bis(3-aminopropyl)ethylenediamine)]$(ClO_4)_2$ in MeCN, with K_f values of 645 M^{-1}, 9.52 M^{-1}, 37.2 M^{-1}, and 6.00 M^{-1}, respectively. The host solid **2** binds selectively PhOH over PhCl and PhBr, showing that hydrogen bonding interaction between the host and guest plays an important role in the selectivity.

Introduction

The preparation of metal-organic open frameworks is one of the most attractive subjects in the current scientific community since they lie at the forefront of new materials that may be applied to adsorption and separation processes [1–3], ion exchange [4], catalysis [5], and sensor technology [6]. However, porous solids with large voids and high framework stability are still rare [2, 7] due to the interpenetration and the irreversible collapse of the structure upon removal of the guest molecules. Some metal-organic open-frameworks show selective guest binding with organic guests [8, 9]. The binding with transition metal complexes, however, is relatively unexplored. Metal ions included in the large channels or cavities might be fabricated into metal clusters, catalysts, and nanoparticles. Encapsulation of toxic heavy metal ions in porous materials is also useful in environmental chemistry [10].

We have constructed various supramolecular networks by using macrocyclic complexes as metal building blocks [3, 9, 11]. Previously, we reported the molecular floral lace, $[Ni(C_{10}H_{24}N_4)(H_2O)_2]_3[BTC]_2{\cdot}24H_2O$ (**1**), which was assembled from nickel(II) cyclam complex (cycalm = $C_{10}H_{24}N_4$) and 1,3,5-benzenetricarboxylate (BTC^{3-}) in water [3]. In this structure, the nickel(II) complex binds two water molecules at the axial sites, which form hydrogen bonds with carboxylate oxygen atoms of BTC^{3-} to give rise to a 3-D structure generating 1-D channels. In this framework, positively charged inorganic and negatively charged organic layers are packed alternately with no open space in the side direction of the 1-D channels. The molecule showed selective binding of glucose vs maltose. Now, we report a new metal-organic open framework, $[Ni(C_{10}H_{26}N_6)]_3[BTC]_2{\cdot}18H_2O$ (**2**), which is self-assembled from the nickel(II) hexaaza macrocyclic complex $[Ni(C_{10}H_{26}N_6)]^{2+}$ and BTC^{3-} in DMF/water mixture. Since the nickel(II) hexaaza macrocyclic complex has smaller affinity for water binding at the axial sites compared with that of cyclam [12], nickel(II) ion is directly coordinated to BTC^{3-} in **2**. The stoichiometry of Ni^{2+}: BTC^{3-} is 3:2, which gives rise to a honeycomb-like 2-D network. In this paper, we report the self-assembly and X-ray structure of the new metal-organic open-framework **2**, and the guest binding of **1** and **2** with various organic and inorganic molecules.

* Supplementary data relating to this article are deposited with the British Library as Supplementary Publication No. SUP 82295 (19 pp.).

** Author for correspondence.

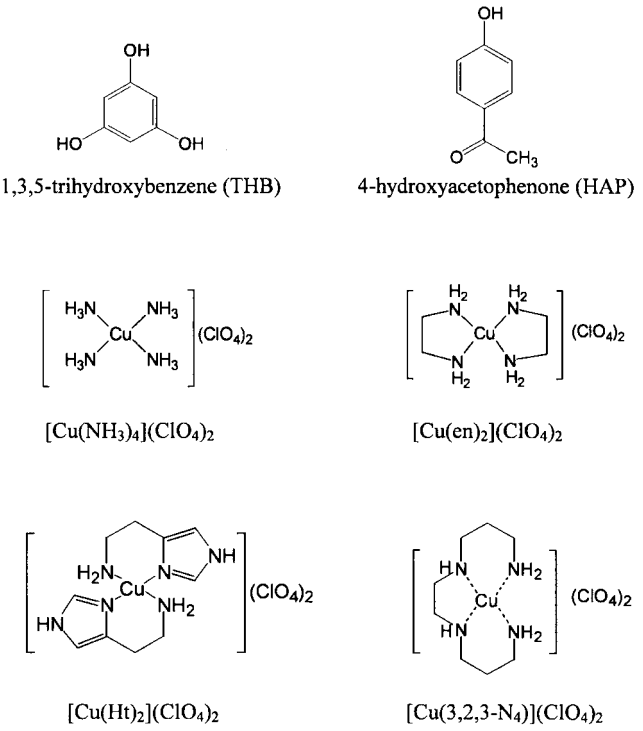

Chart 1.

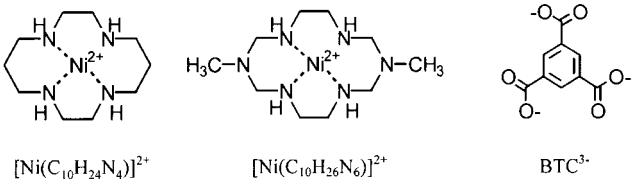

Chart 2.

Experimental

General procedures

All chemicals and solvents used in the syntheses were of reagent grade and were used without further purification. For the guest binding, MeCN solvent was distilled over P_2O_5 and *n*-hexane was purified by fractional distillation. All solvents were dried with molecular sieves prior to use. Infrared spectra were recorded with a Perkin Elmer 2000 FT-IR spectrophotometer. Elemental analyses were performed by the analytical laboratory of Seoul National University. UV/vis diffuse reflectance spectra were recorded with a Cary 300 Bio UV/vis spectrophotometer. Thermogravimetric analysis (TGA) and differential thermal analysis (DTA) were obtained at a scan rate 10 °C min^{-1} using a Rigaku Tas-100 system. X-ray powder diffraction data (XRPD) were recorded on a Mac Science M18XHF-22 diffractometer at 50 kV and 100 mA for Cu Kα (λ = 1.54050 Å) with a scan speed of 5° min^{-1} and a step size of 0.02° in 2θ. Gas chromatographic (GC) experiments were conducted by using a HP 6890 Series GC system which was fitted with a 30 m × 0.25 mm × 0.25 μm crosslinked polydimethylsiloxane capillary column and interfaced with a GC ChemStation. The column temperature was programmed from 110 °C (3 min) to 230 °C (1 min) at the rate of 120 °C min^{-1} for MeOH, 130 °C (3 min) to 230 °C (1 min) at the rate of 100 °C min^{-1} for PhOH (for 1), 120 °C (1 min) to 180 °C (1 min) at the rate of 60 °C min^{-1} and then to 220 °C (1 min) at the rate of 40 °C min^{-1} for THB and HAP (for the chemical formula, see Chart 1), and 80 °C (3 min) to 200 °C (3 min) at the rate of 120 °C min^{-1} for PhX (X = OH, Br, Cl for **2**). A flame ionization detector was used.

Table 1. Crystallographic data for **2**

	2
Empirical formula	$Ni_3C_{48}H_{120}N_{18}O_{30}$
Fw	1605.76
Space group	$P2_1/c$, Monoclinic
a, Å	9.4784(1)
b, Å	28.3558(2)
c, Å	16.8801(2)
α, deg	90
β, deg	101.836(1)
γ, deg	90
V, $Å^3$	4440.36(8)
Z	2
ρ_{calc}, g cm^{-3}	1.201
T, °C	20(2)
μ, mm^{-1}	0.706
R_1[a], (4σ data)	0.0716
wR_2[b], (4σ data)	0.2029

[a] $R_1 = \Sigma||F_o| - |F_c||/\Sigma|F_o|$.
[b] $wR_2(F^2) = [\Sigma w(F_o^2 - F_c^2)^2/\Sigma w(F_o^2)^2]^{1/2}$.

X-ray diffraction measurements

A single crystal of **2** was sealed in a glass capillary together with the mother liquor. X-ray data were collected at room temperature using graphite monochromated Mo Kα-radiation on an Enraf-Nonius CAD4 diffractometer. The orientation matrix and unit cell parameters were determined from 25 machine-centered reflections with $2.9° < 2\theta < 49°$. Axial photographs were used to verify the unit cell choice. Data were corrected for Lorentz and polarization effects. No absorption correction was made. All calculations were carried out on a personal computer by using SHELXS-86 [13] and SHELXL-93 [14] programs. The structure was solved by the Patterson method. All non-hydrogen atoms were refined anisotropically. All hydrogen atoms were positioned geometrically and refined using a riding model. The crystallographic data are summarized in Table 1, and the selected bond distances and angles are in Table 2.

*Synthesis of $[Ni(C_{10}H_{24}N_4)(H_2O)_2]_3[BTC]_2{\cdot}24H_2O$ **1***

The compound was prepared according to the method reported previously [3].

Synthesis of $[Ni(C_{10}H_{26}N_6)](CF_3SO_3)_2$

The compound was prepared according to the method reported previously [12].

Table 2. Selected bond length [Å] and angles [°] for **2**

Ni1-N2	2.055(5)	N5-C7	1.477(8)
Ni1-N3	2.048(5)	N5-C8	1.480(7)
Ni1-O1	2.151(3)	N6-C9	1.484(9)
Ni2-N5	2.055(5)	N6-C10	1.485(8)
Ni2-N6	2.043(5)	N7-C10	1.419(10)
Ni2-N8	2.0557(5)	N7-C12	1.451(10)
Ni2-N9	2.053(4)	N7-C11	1.465(10)
Ni2-O3	2.195(3)	N8-C13	1.469(9)
Ni2-O5′	2.168(3)	N8-C12	1.472(8)
N1-C2	1.442(10)	N9-C15	1.467(7)
N1-C1	1.487(10)	N9-C14	1.478(8)
N2-C3	1.467(8)	O1-C16	1.260(6)
N2-C2	1.467(10)	O2-C16	1.249(6)
N3-C4	1.474(8)	O3-C17	1.252(6)
N3-C5	1.509(9)	O4-C17	1.252(6)
N4-C15	1.434(8)	O5-C18	1.249(6)
N4-C7	1.443(9)	O6-C18	1.245(6)
N4-C6	1.447(10)		
N3-Ni1-N2	85.5(2)	N5-Ni2-O3	0.1(2)
N3-Ni1-N2″	94.5(2)	N8-Ni2-O3	89.6(2)
N3″-Ni1-N2″	85.5(2)	O5′-Ni2-O3	179.07(15)
N2″-Ni1-O1	86.1(2)	C16-O1-Ni1	134.0(3)
N6-Ni2-N9	179.3(2)	C17-O3-Ni2	131.9(3)
N6-Ni2-N5	86.6(2)	C18-O5-Ni2‴	133.9(3)
N9-Ni2-N5	94.1(2)	O2-C16-O1	125.4(5)
N6-Ni2-N8	93.6(2)	O2-C16-C19	117.6(4)
N9-Ni2-N8	85.7(2)	O1-C16-C19	117.0(4)
N5-Ni2-N8	79.6(2)	O3-C17-O4	125.3(5)
N6-Ni2-O5′	87.23(15)	O3-C17-C21	117.8(4)
N9-Ni2-O5′	92.72(15)	O4-C17-C21	116.9(4)
N5-Ni2-O5′	89.0(2)	O6-C18-O5	125.6(5)
N8-Ni2-O5′	91.3(2)	O6-C18-C23	117.5(4)
N6-Ni2-O3	92.6(2)	O5-C18-C23	117.0(4)
N9-Ni2-O3	87.48(15)		

[a] Symmetry transformations used to generate equivalent atoms: prime, $x+1, -y+1/2, z+1/2$; double prime, $-x, -y, -z$; triple prime, $x-1, -y+1/2, z-1/2$.

*Synthesis of [Ni($C_{10}H_{26}N_6$)]$_3$[BTC]$_2$·18H_2O **2***

To a warm (50 °C ∼ 60 °C) DMF solution (3 mL) of [Ni($C_{10}H_{26}N_6$)](CF_3SO_3)$_2$ (0.300 g), an aqueous solution (3 mL) of Na_3BTC (0.101 g) was added dropwise. The mixture was allowed to stand at room temperature for several days until pale purple plate-like crystals formed. The crystals were filtered off, washed briefly with MeOH, and dried in air. Yield: 87%. Anal. Calcd for $Ni_3C_{48}H_{126}N_{18}O_{33}$: C, 34.73; H, 7.65; N, 15.19. Found: C, 34.22; H, 5.32; N, 15.03. FT-IR (Nujol mull; cm^{-1}): 3386 (br), 3288, 3168, 1607, 1564. UV/vis (diffuse reflectance spectrum, λ_{max}): 507 nm.

*Binding of **1** and **2** with organic guests*

The formation constant (K_f) for the host–guest complexes formed between a binding site (BS) of the insoluble host and a guest molecule (G) can be defined as k_{ad}/k_{de} (Equation (1)) by analogy with the Langmuir isotherm for adsorption of gas molecules on solid surfaces [3,15].

$$\mathrm{BS} + \mathrm{G} \underset{k_{de}}{\overset{k_{ad}}{\rightleftharpoons}} \mathrm{BS{\cdot}G}$$

$$K_f = \frac{k_{ad}}{k_{de}} = \frac{[\mathrm{BS{\cdot}G}]}{[\mathrm{BS}][\mathrm{G}]}. \tag{1}$$

If θ is defined as the fractional coverage,

$$\theta = \frac{[\mathrm{BS{\cdot}G}]}{[\mathrm{BS}]_0} = \frac{[\mathrm{G}]}{\left([\mathrm{G}] + \frac{1}{K_f}\right)}$$

then

$$[\mathrm{BS{\cdot}G]}/\omega = \frac{([\mathrm{BS}]_0/\omega)[\mathrm{G}]}{\left([\mathrm{G}] + \frac{1}{K_f}\right)}, \tag{2}$$

where ω is amount of host solid per unit volume of the solution (mg/mL) [9].

According to Equation (2), the plots of the concentration of G bound to BS ([BS·G]) against [G] were made and the K_f and $[\mathrm{BS}]_0$ values were estimated by the analysis of the data. In the experiment, the total concentration of guest ($[\mathrm{G}]_0$) was varied to keep the θ values ranging from 20–80%.

In fitting the experimental data of MeOH binding to **1**, we modified BET Equation (3), which describes a model for multilayer gas adsorption [16, 17].

$$n = n_m \frac{c(p/p^0)}{1-(p/p^0)} \frac{1-(n+1)(p/p^0)^N + n(p/p^0)^{N+1}}{1+(c-1)(p/p^0) - c(p/p^0)^{N+1}}. \tag{3}$$

In Equation (3), n is the adsorbed amount (cm^3/g, mol/g, μg/g, etc.), n_m is the monolayer capacity, p is the equilibrium pressure, p^0 is the saturation vapor pressure, and c is a coefficient related to the difference of adsorption energies in the first and upper adsorbed layers, measured in units k_BT (k_B = Boltzmann constant), N is the maximum number of molecular layers on the surface. Defining the relative pressure x ($x = p/p^0$), the BET Equation (3) becomes a more compact, two parameter form (4), which is eventually reduced to the canonical form in the limit for $n \to +\infty$.

$$n = n_m \frac{cx}{(1-x)(1+(c-1)x)}. \tag{4}$$

The BET Equation (4) was modified to Equation (5) by introducing the coefficient k which has a value less than unity, to obtain better agreement with the experimental isotherm data in the multilayer region.

$$n = n_m \frac{ckx}{(1-kx)(1+(c-1)kx)}. \tag{5}$$

The modified BET Equation (5) was made on the assumption that the number of molecular layers at saturation pressure p^0 was finite, even on an open surface [16]. Equation (5) can be converted to Equation (6) by replacing n to $[\mathrm{BS{\cdot}G}]/\omega$, n_m to $[\mathrm{BS}]_0/\omega$, and x to $[\mathrm{G}]/[\mathrm{G}]_{max}$ ($[\mathrm{G}]_{max}$ is the maximum equilibrium concentration).

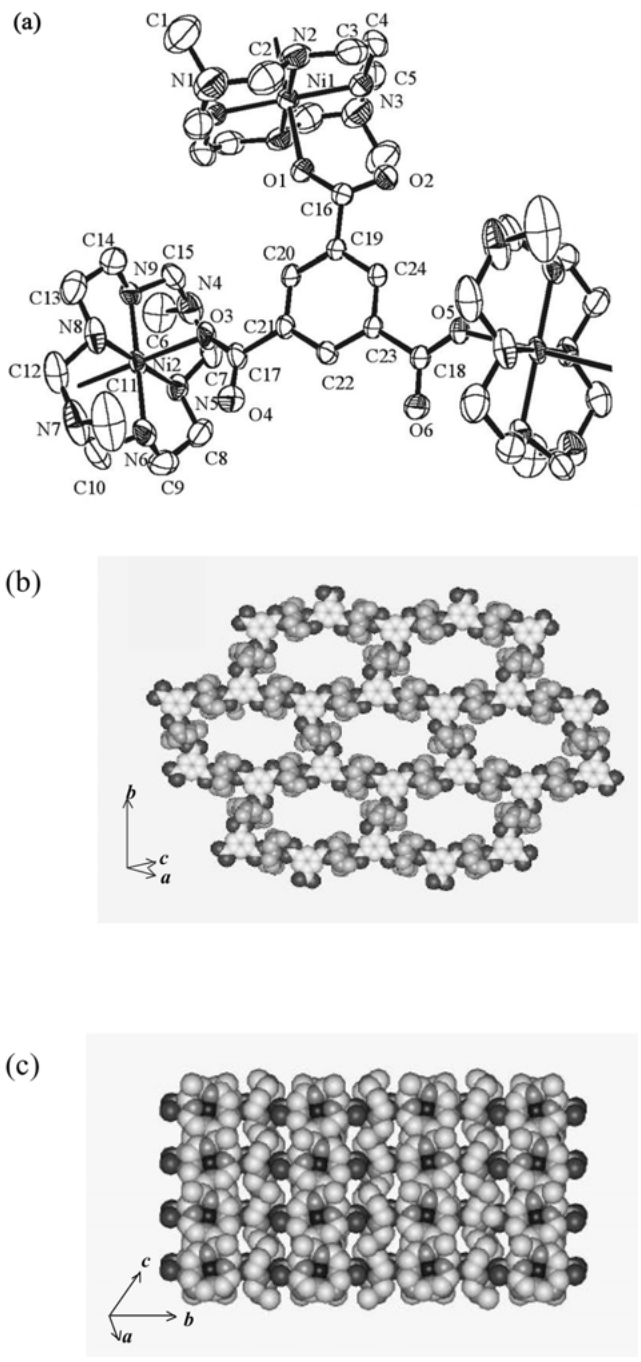

Figure 1. X-ray structure of **2**. (a) An ORTEP view with atomic numbering scheme. The atoms are represented by 50% probable thermal ellipsoids. (b) CPK representation showing the topview of a 2-D layer of **2**. (c) CPK representation showing the sideview of **2**. The accessible channel size is ca. 12.5×6.67 Å^2.

$$[\mathrm{BS{\cdot}G}]/\omega = ([\mathrm{BS}]_0/\omega)\frac{ckx}{(1-kx)(1+(c-1)kx)}. \quad (6)$$

With the experimental data, the plots of the concentration of G bound to BS ([BS·G]) against [G] were made, and c and $[\mathrm{BS}]_0$ values were estimated by the analysis of the data according to Equation (6).

Pale pink crystals of **1** and **2** were ground in a mortar until they became a microcrystalline powder, dried at 85 °C for 1 h for **1** and 100 °C for 1 h for **2**, and then kept in a desiccator. Host solids were immersed in the dilute solution of a guest and the time-dependent guest adsorption was monitored by GC to check the attainment of equilibrium. The solid **1** (20–30 mg), whose weight was measured exactly, was immersed for 4 h in the toluene solutions (2.00 mL) containing PhOH and MeOH, respectively. It was also immersed in EtOH/toluene (v/v = 1/4) solutions containing THB for 3 h and HAP for 4.5 h, respectively. The solid **1** did not bind toluene and it bound a negligible amount of EtOH, as measured by GC as shown in Figure S1. The initial concentrations of PhOH, MeOH, THB, and HAP were varied from $4.70\times10^{-3}-2.35\times10^{-1}$ M, $1.02\times10^{-2}-4.29\times10^{-1}$ M, $4.35\times10^{-3}-1.80\times10^{-1}$ M, $3.30\times10^{-3}-1.97\times10^{-1}$ M, respectively, to keep the percent saturation values (θ) at 20–80%. Similarly, solid **2** (20–30 mg) was immersed in the *n*-hexane solutions (2.00 mL) containing PhOH, PhBr, and PhCl, respectively, for 12 h at 25 °C. The concentrations of PhOH, PhBr, and PhCl were varied from $4.53 \times 10^{-3} - 3.63 \times 10^{-1}$ M, $11.48 \times 10^{-3} - 1.18 \times 10^{-1}$ M, $6.62 \times 10^{-3} - 4.63 \times 10^{-1}$ M, respectively. The change in the concentration of the organic guest was measured by GC using dodecane as the internal standard.

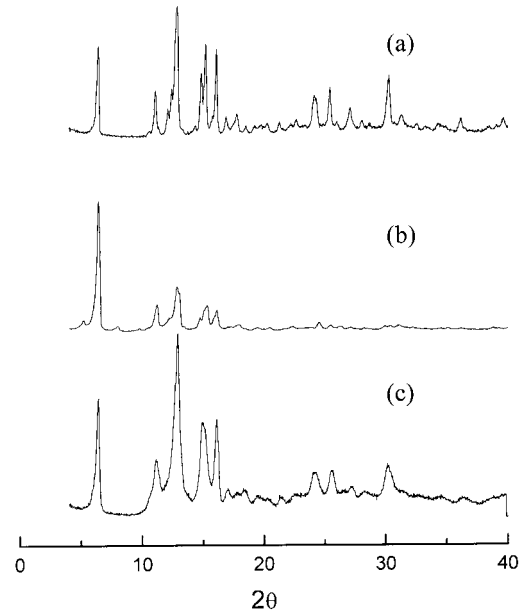

Figure 2. XRPD patterns of (a) original solid **2**, (b) solid **2** heated to 100 °C at a rate of 3.2 °C/min, (c) solid b after exposure to water vapor for 12 h.

*Guest exchange of **1** with inorganic guests*

In this experiment, host **1** as prepared was used instead of the desolvated sample. Freshly prepared pink crystals of **1** were ground in a mortar until they became a microcrystalline powder. The solid sample (10 mg) whose weight was accurately measured was immersed in the MeCN solutions (5.00 mL) containing $[Cu(NH_3)_4](ClO_4)_2$, $[Cu(en)_2](ClO_4)_2$, $[Cu(Ht)_2](ClO_4)_2$, and $[Cu(3,2,3\text{-}N_4)](ClO_4)_2$, respectively, for 8 days at 25 °C. The initial concentrations of the above metal complexes were varied from $3.00\times10^{-3}-2.50\times10^{-2}$ M, $3.00\times10^{-3}-5.01\times10^{-2}$ M, $3.00\times10^{-3}-2.50\times10^{-2}$

M, and $1.01 \times 10^{-3} - 5.06 \times 10^{-2}$ M, respectively, to keep the saturation values at 20–80%. The absorbance changes of the complexes were measured spectrophotometrically.

Results and discussion

*Self-assembly, property, and X-ray structure of **2***

In the open-framework structure of **1**, two water molecules coordinate nickel(II) cyclam at the axial sites and they are hydrogen bonded to BTC^{3-}, which generates the 3-D structure with 1-D channels of effective diameter 10.3 Å [3]. However, the azacyclam complex $[Ni(C_{10}H_{26}N_6)]^{2+}$ has a much smaller equilibrium constant (K) than $[Ni(cyclam)]^{2+}$ for water binding [12] and the self-assembly between $[Ni(C_{10}H_{26}N_6)]^{2+}$ and BTC^{3-} in DMF/water leads to direct coordination of BTC^{3-} to nickel(II) ion, which gives rise to a 2-D network with brick-wall structure. The supramolecule **2** is insoluble in any solvent except H_2O.

$$[Ni(Mac)]^{2+} + 2H_2O \overset{K}{\rightleftharpoons} [Ni(Mac)(H_2O)_2]^{2+}.$$

An ORTEP view of the fundamental building unit of **2** is shown in Figure 1. Table 2 shows the selected bond distances and angles. The nickel(II) ion is coordinated with four secondary amine donors of the macrocycle as well as two oxygen atoms of BTC^{3-} ions. The average Ni–N and Ni–O bond distances are 2.052(3) Å and 2.171(2) Å, respectively. Since each nickel(II) ion is coordinated with two BTC^{3-} ions and each BTC^{3-} binds three nickel(II) macrocyclic units, the stoichiometry of the network is $Ni^{2+}/BTC^{3-} = 3{:}2$, which generates 2-D layers extending along the $[10\bar{2}]$ plane. The metal-metal distances around BTC^{3-} are Ni1···Ni2 = 8.178(1) Å, Ni2···Ni2($x-1, -y+1/2, z-1/2$) = 11.327(0) Å, and Ni1···Ni2($x-1, -y+1/2, z-1/2$) = 10.084(1) Å. In the 2-D layer, six Ni(II) macrocyclic complexes and six BTC^{3-} form a rectangular ring (27.8×14.5 Å^2), which is a basic motif of the framework (Figure 1b). The layers are slightly offset-stacked so that the channels created by the stacked layers have dihedral angles of 38.8° relative to the 2-D layers. The channels run parallel to the *a* axis. The accessible void of the channel is 12.5×6.76 Å^2, as estimated from van der Waals surfaces. The interlayer distance is 7.38 Å. The BTC^{3-} ion is almost planar, since dihedral angles between benzene and each carboxylate plane of BTC^{3-} are 17.13°, 14.97°, and 11.31°, respectively. The macrocyclic coordination planes are tilted with respect to the benzene plane of the coordinating BTC^{3-} ion with the dihedral angles of 86.9°, 84.7°, and 83.5°, respectively. The channels are filled with guest water molecules that are hydrogen bonded with the host framework through the carbonyl oxygen atoms of BTC^{3-} ions {Ow1···O2 ($-x, y-1/2, -z+1/2$), 2.807 Å; Ow2···O2 ($x+1, -y+1/2, z+1/2$), 2.831 Å; Ow4···O6 ($-x, -y+1, -z$), 2.812 Å; Ow5···O4($x, y, z+1$), 2.844 Å, Ow6···O4($-x, -y+1, -z+1$), 2.845 Å}, the nitrogen atoms of macrocyclic ligand {Ow3···N8($-x, y+1/2, -z+1/2$), 2.941 Å; Ow7···N1($-x, y+1/2, -z+1/2$), 2.888 Å; Ow8···N2($-x, y+1/2, -z+1/2$), 3.031 Å; Ow8···N7(x, y, z), 2.892 Å; OW9···N4($x, -y+1/2, z+1/2$), 2.949 Å}, and other guest water molecules {Ow1···Ow6(x, y, z), 2.803 Å; O5W···OW3′($-x, -y+1, -z+1$), 2.876 Å}. The void volume of the cavities in a unit cell is 1794.4 Å^3 (40.5%) as estimated by PLATON [18].

Molecular-based materials that are stable even after removal of guests are important in view of the development of a new class of porous substances. TGA data for crystalline sample **2** indicate that all guest water molecules are removed at 98 °C, and it can be further heated to 240 °C without decomposition. XRPD patterns of the dried solids are compared with those of **2** in Figure 2. When crystal **2** was heated at 100 °C for 1 h, some lines were slightly broadened but their positions were unaltered compared with those of **2**. When water vapor was diffused into this dried solid, XRPD patterns the same as those of the original crystal were regenerated.

*Binding of **1** and **2** with organic guest molecules*

When desolvated host solid **1** (in powder form) was immersed in toluene solutions containing PhOH and MeOH, respectively, the concentration of the organic compounds changed as measured by GC. With a measured amount of the host solid, concentration changes of the organic guests were measured with various initial concentrations of the guest ($[G]_0$), and the data were fitted to Equation (2) according to Ref. [9] to obtain K_f values. In contrast to MeOH, EtOH was slightly included in solid **1**. The binding studies with THB and HAP were carried out in EtOH/toluene (v/v = 1/4) solution since they are not soluble in toluene. The plots of $[BS{\cdot}G]/\omega$ (the concentration of G bound to BS) against [G] for the binding of **1** with various organic guests are illustrated in Figure 3. Similarly, when desolvated host solid **2** (in powder form) was immersed in the *n*-hexane solutions of PhOH, PhCl, and PhBr, respectively, the concentration of the organic compounds was reduced. The plots of $[BS{\cdot}G]/\omega$ against [G] for solid **2** are illustrated in Figure 4. The values of binding constants ($\log K_f$) and the number of binding site ($[BS]_0/\omega$) of host solids **1** and **2** for various guest molecules are summarized in Table 3. Estimated organic guest sizes are $5.2 \times 4.2 \times 4.0$ Å^3 for MeOH, $6.0 \times 4.2 \times 4.0$ Å^3 for EtOH, $8.0 \times 6.6 \times 3.4$ Å^3 for PhOH, $9.3 \times 8.8 \times 3.4$ Å^3 for THB, $11.2 \times 6.9 \times 4.4$ Å^3 for HAP, $8.7 \times 6.9 \times 4.0$ Å^3 for PhBr, and $8.5 \times 6.9 \times 4.0$ Å^3 for PhCl.

Although microporous materials generally exhibit a Langmuir curve for adsorption, host solid **1** (desolvated) shows various binding curves depending on the type of guest (Figure 3). The binding of MeOH to **1** shows a plateau at the low concentration range and increases abruptly in the higher concentration range, which yields a type II isotherm curve according to the BDDT classification [16]. The solid line in Figure 3a is obtained by fitting the data to the modified BET Equation (6) described in the experimental section. The best fit parameters are $k = 0.84$, $c = 55.9$ and $[BS]_0/\omega = 3.05 \times 10^{-3}$ mol/g. If $[BS]_0/\omega$ is estimated from the first plateau by using Equation (2) (insert in Figure 3a), it is 4.62×10^{-3} mol/g, which corresponds to 6 molecules of

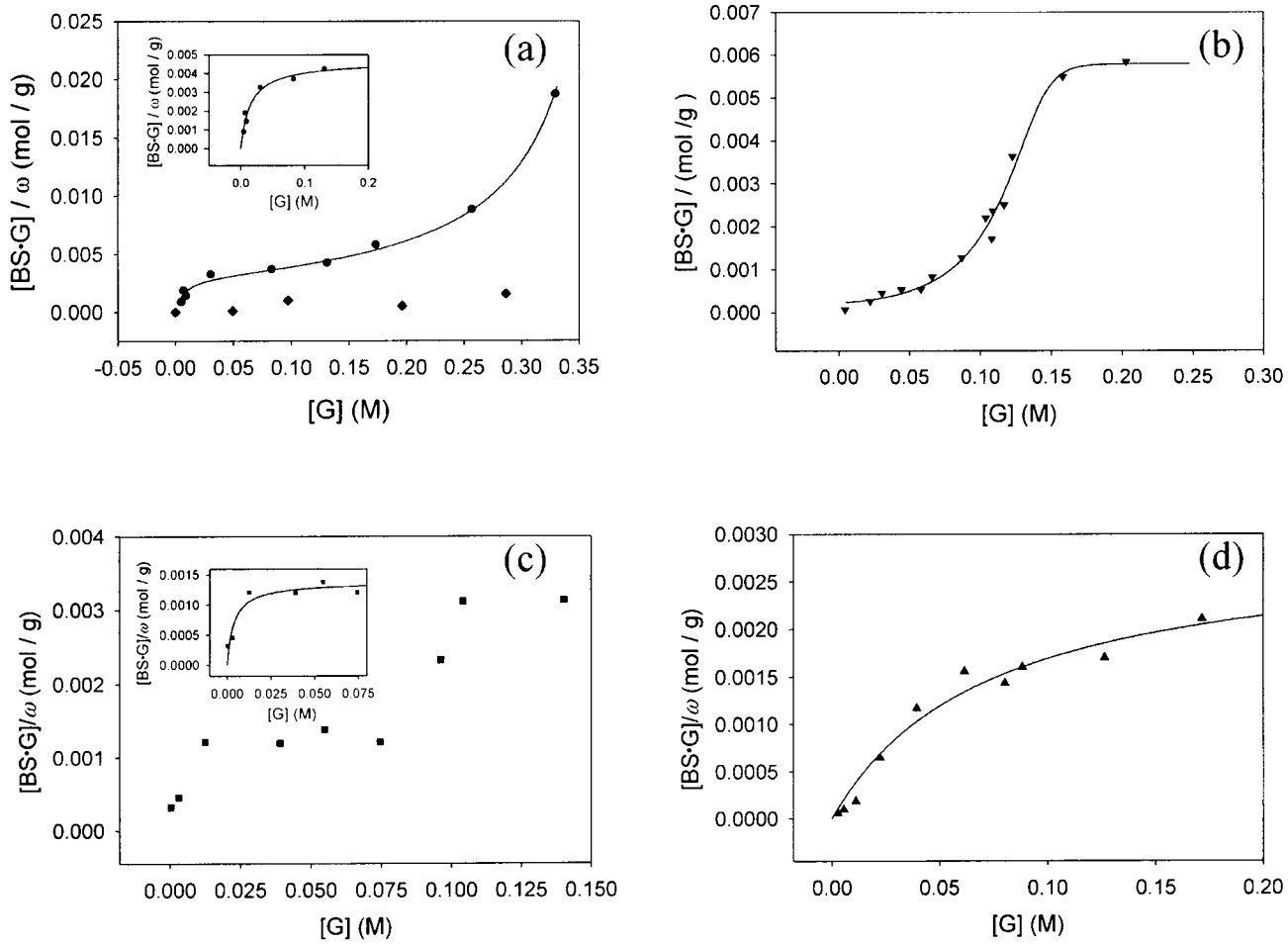

Figure 3. Binding of host solid **1** with various guests. (a) MeOH (●) and EtOH (♦) in toluene. The solid lines indicate the best fit curves to Equation (6) and Equation (2) (insert), respectively. (b) PhOH(▼) in toluene, (c) THB (■) in EtOH/toluene (v/v = 1/4) solution. The solid line indicates the best fit curve to Equation (2) (insert), (d) HAP (▲) in EtOH/toluene (v/v = 1/4) solution.

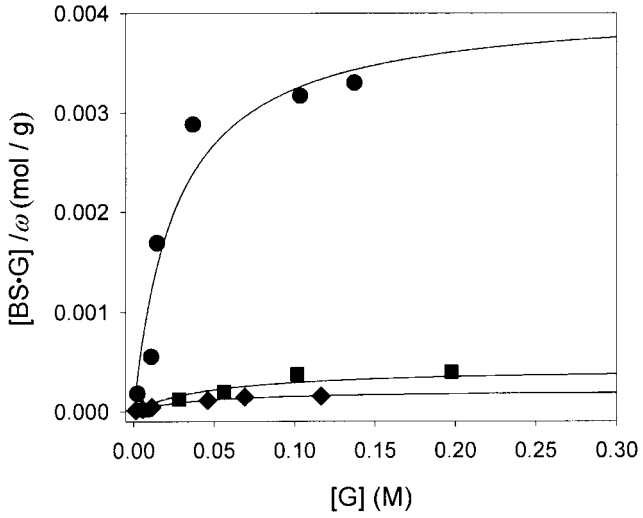

Figure 4. Binding of host solid **2** with PhOH (●), PhBr (■), and PhCl (♦) in *n*-hexane.

MeOH (ca. 524 Å^3) per unit formula of host. This roughly agrees with the elemental analysis obtained for the guest included solid, which indicates 7 mol of MeOH inclusions per unit formula of host. However, in the higher concentration, MeOH molecules adsorb on the external surface of host solid by the MeOH–MeOH interactions.

The binding of PhOH to **1** shows a sigmoid curve, which is a type V isotherm according to the BDDT classification. It reaches a maximum [BS·G]/ω value (ca. 1360 Å^3) that corresponds to 7.6 mol of PhOH per formula unit of host (Figure 3b). Since PhOH molecules are well solvated by toluene, PhOH dissolved in toluene may prefer not to be included into the micropores of solid **1** in the low concentration range. However, once PhOH is bound to the host, further binding of PhOH is promoted by hydrogen bonding and π–π stacking interactions between PhOH molecules [19].

The binding of THB to **1** shows a similar curve to that of PhOH except that there is a steep uptake in the low THB concentration range, which indicates strong affinity of THB to the hydrophilic channels (Figure 3c). The binding constant K_f estimated from the first plateau is 259 M^{-1} (insert in Figure 3c), which is the largest among those for other organic guests. This must be attributed to the fact that THB contains three hydroxyl groups that can be involved in the hydrogen bonding interactions with the host while MeOH, PhOH, and HAP have only one. The interactions between the guest molecules seem to make the second plateau appear

Table 3. Inclusion of host solid with various organic/inorganic guest molecules

Host	Guest	log K_f, M^{-1}	$[BS]_0/\omega$, mmol/g	Maximum amount of guest (mol) bound per unit formula of host solid
1	MeOH[a]	1.82 ± 0.11	4.62 ± 0.35	6.00 ± 0.458
	PhOH[a]	–	–	7.6[c]
	THB[a]	2.41 ± 0.21	1.38 ± 0.12	1.79 ± 0.16, 4.0[c]
	HAP[a]	1.14 ± 0.12	2.91 ± 0.36	3.78 ± 0.46
	$[Cu(NH_3)_4](ClO_4)_2$[b]	2.81 ± 0.03	1.90 ± 0.00	3.30 ± 0.00
	$[Cu(en)_2](ClO_4)_2$[b]	0.98 ± 0.14	3.70 ± 0.90	6.41 ± 0.85
	$[Cu(Ht)_2](ClO_4)_2$[b]	1.57 ± 0.37	0.90 ± 0.50	1.56 ± 0.87
	$[Cu(3,2,3\text{-}N_4)](ClO_4)_2$[b]	0.78 ± 0.65	1.30 ± 1.50	2.25 ± 2.60
2	PhOH[a]	1.58 ± 0.20	4.09 ± 0.61	5.24 ± 0.78[a]

[a] Dried host solids were used in the binding experiment. $[Ni(C_{10}H_{24}N_4)(H_2O)_2]_3[BTC]_2$ for **1** and $[Ni(C_{10}H_{26}N_6)]_3[BTC]_2$ for **2**.
[b] Host solid as prepared, $[Ni(C_{10}H_{24}N_4)(H_2O)_2]_3[BTC]_2 \cdot 24H_2O$, was used.
[c] Estimated from the observed maximum $[BS{\cdot}G]/\omega$ value in Figure 3.

at the $[BS{\cdot}G]/\omega$ value corresponding to 4.0 mol (ca. 1120 Å^3) of THB per formula unit of host solid.

The binding of host **1** with HAP shows a Langmuir curve (Figure 3d). The estimated $[BS]_0/\omega$ value corresponds to 3.8 mol (ca. 1280 Å^3) of HAP per formula unit of host solid. This roughly agrees with the elemental analysis result for the guest included host solid, indicating that 4.2 mol of HAP were bound per unit formula of host.

As seen in the binding curves of PhOH, THB and HAP guest molecules with host solid **1**, they show saturation of binding at the high concentration of guest, which does not happen in the case of MeOH. This may be attributed to the hydrogen bonding and π–π stacking interactions between the guest molecules.

The total volumes of guest molecules that are able to bind to the unit formula of host **1**, as estimated from the $[BS{\cdot}G]/\omega$ values, are 524 Å^3 for MeOH, 1360 Å^3 for PhOH, 1120 Å^3 for THB, and 1280 Å^3 for HAP. These values are larger than the total cavity volume (789 Å^3) of the host solid **1**, which is estimated by PLATON [18], except in the case of MeOH. It means that the guests are included between the layers as well as in the cavities.

The host solid **2** (desolvated) binds selectively PhOH over PhBr or PhCl, showing a characteristic monolayer adsorption curve (Figure 4). This indicates that hydrogen bonding interaction between the host and the guest plays a major role in the guest binding. The estimated $[BS]_0/\omega$ value of PhOH corresponds to 5.2 mol (ca. 936 Å^3) per formula unit of host solid **2**, which roughly agrees with the elemental analysis result for the guest included host solid indicating that 6.0 mol of PhOH was bound per unit formula of host. This is comparable to the total cavity volume (899 Å^3) of the host solid **2** estimated by PLATON [18].

The host–guest complexes were isolated and characterized by elemental analysis and IR spectra (Table S7 and Figures S2–S6).

*Binding of **1** with coordination compounds*

When crystal **1** was immersed in the MeCN solutions of $[Cu(NH_3)_4](ClO_4)_2$, $[Cu(en)_2](ClO_4)_2$, $[Cu(Ht)_2](ClO_4)_2$, and $[Cu(3,2,3\text{-}N_4)](ClO_4)_2$, respectively, the pale pink color of the host solid changed to blue, green, blue, violet, blue-violet, violet, respectively, and the color intensity of the copper(II) solution was reduced. The diffuse reflectance spectra of the guest bound solids show λ_{max} at 649, 529, 736, and 515 nm, respectively. (Figures S6–S9). The color of the guest-bound solid changed to pale pink when the solid was immersed again in cold water, indicating that binding of the guest complex was reversible. To obtain the K_f and $[BS]_0/\omega$ values for the formation of host-guest complexes, the absorbance changes of the copper(II) solutions were measured by varying the initial concentration of the guests ($[G]_0$) with the measured amount of the host solid. The plots of $[BS{\cdot}G]/\omega$ (the concentration of G bound to BS) against [G] are illustrated in Figure 5. The values of log K_f and $[BS]_0/\omega$ are summarized in Table 3. The data indicate that the host solid **1** binds guests in the order of K_f, $[Cu(NH_3)_4](ClO_4)_2 \gg [Cu(Ht)_2](ClO_4)_2 > [Cu(en)_2](ClO_4)_2 > [Cu(3,2,3\text{-}N_4)](ClO_4)_2$. Therefore, this selectivity should depend on the ability of guest for hydrogen bond formation with carbonyl oxygen atoms of BTC^{3-} directing toward the channels. Since the host consists of al-

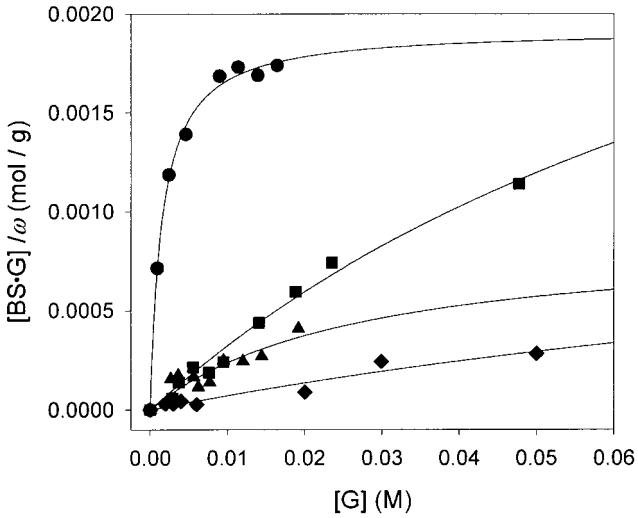

Figure 5. Binding of host solid **1** with various copper(II) complexes in MeCN. $[Cu(NH_3)_4](ClO_4)_2$ (●), $[Cu(en)_2](ClO_4)_2$ (■), $[Cu(Ht)_2](ClO_4)_2$ (▲), and $[Cu(3,2,3\text{-}N_4)](ClO_4)_2$ (♦).

ternately packed positively charged and negatively charged layers, the positively charged guest complex will be included in the cavities of the BTC^{3-} layer and negative anions will be included in the macrocyclic layer. The estimated sizes of the cationic complexes are 5.1 × 5.1 × 4.0 Å^3 for $[Cu(NH_3)_4](ClO_4)_2$, 6.5 × 9.6 × 4.4 Å^3 for $[Cu(en)_2](ClO_4)_2$, 12 × 11 × 4.0 Å^3 for $[Cu(Ht)_2](ClO_4)_2$, and 11 × 9.8 × 5.5 Å^3 for $[Cu(3,2,3\text{-}N_4)](ClO_4)_2$. The diameter of ClO_4^- is estimated as 5.8 Å. The fact that host solid **1** selectively binds the $[Cu(NH_3)_4]^{2+}$ complex implies that the binding of the complex takes place in the channels rather than by adsorption on the solid surface. The host–guest complexes were isolated and characterized by elemental analyses and IR spectra (Table S7 and Figures S7–S10). In the IR spectra of **1** with copper(II) guest complex inclusions, primary amine peaks of the copper(II) complexes were observed together with the anion peaks.

In conclusion, we have constructed a new 2-D network **2**, which has a completely different structure from that of **1**, by employing the nickel(II) hexazamacrocyclic complex and BTC^{3-}. Binding of **1** with PhOH, MeOH, THB, and HAP showed diverse binding curves depending upon the guest molecules due to the interactions with the host as well as the interactions between the guests. The host solid **2** binds PhOH selectively over PhBr and PhCl. Host solid **1** also differentiates $[Cu(NH_3)_4](ClO_4)_2$, $[Cu(en)_2](ClO_4)_2$, $[Cu(Ht)_2](ClO_4)_2$, and $[Cu(3,2,3\text{-}N_4)](ClO_4)_2$. The binding with the copper(II) complexes were reversible. Because of the selective guest binding ability, the host solids **1** and **2** may be applied as molecular filters.

Acknowledgements

This work was supported by the Korea Science and Engineering Foundation (R01-1999-00041) and the Center for Molecular Catalysis.

References

1. H. Li, M. Eddaoudi, M. O'Keeffe, and O.M. Yaghi: *Nature* **402**, 276 (1999).
2. S.-I. Noro, S.M. Kitagawa, Kondo, and K. Seki: *Angew. Chem. Int. Ed.* **39**, 2082 (2000).
3. H.J. Choi, T.S. Lee, and M.P. Suh: *Angew. Chem. Int. Ed.* **38**, 1405 (1999).
4. (a) K.S. Min and M.P. Suh: *J. Am. Chem. Soc.* **122**, 6834 (2000). (b) O.M. Yaghi and H. Li: *J. Am. Chem. Soc.* **118**, 295 (1996).
5. (a) J. S. Seo, D.-M. Whang, H.-Y. Lee, S. I. Jun, J.-H. Oh, Y.J. Jeon, and K.-M. Kim: *Nature* **404**, 982 (2000). (b) T. Sawaki and Y. Aoyama: *J. Am. Chem. Soc.* **121**, 4793 (1999).
6. (a) M. Albrecht, M. Lutz, A.L. Spek, and G. van Koten: *Nature* **406**, 970 (2000). (b) J.A. Real, E. Andrés, M.C. Muñoz, M. Julve, T. Granier, A. Bousseksou, and F. Varret: *Science* **268**, 265 (1995).
7. S. S.-Y. Chui, S. M.-F. Lo, J.P.H. Charmant, A.G. Orpen, and I.D. Williams: *Science* **283**, 1148 (1999).
8. (a) O.M. Yaghi, G. Li, and H. Li: *Nature* **378**, 703 (1995). (b) M. Kondo, T. Yoshitomi, K. Seki, H. Matsuzaka, and S. Kitagawa: *Angew. Chem. Int. Ed. Engl.* **36**, 1725 (1997).
9. K.S. Min and M.P. Suh: *Chem. Eur. J.* **7**, 303 (2001).
10. F. Sinner, M.R. Buchmeiser, R. Tessadri, M. Mupa, K. Wurst, and G.K. Bonn: *J. Am. Chem. Soc.* **120**, 2700 (1998).
11. H.J. Choi and M.P. Suh: *J. Am. Chem. Soc.* **120**, 10622 (1998).
12. M.P. Suh: *Advances in Inorganic Chemistry*, **44**, 93 (1997).
13. G.M. Sheldrick: *SHELXS-86. Program for the Solution of Crystal Structures*, University of Göttingen: Göttingen of Germany (1986).
14. G.M. Sheldrick: *SHELXL-93. Program for the Solution of Crystal Structures*, University of Göttingen: Göttingen of Germany (1993).
15. (a) P.W. Atkins: *Physical Chemistry, 4th edn*, Oxford University Press, Oxford, pp. 885–888 (1990). (b) B.-B. Jang, K.-P. Lee, D.-H. Min, and J. Suh: *J. Am. Chem. Soc.* **120**, 12008 (1998). (c) J. Suh and H. S. Park: *J. Polym. Sci. A: Polm. Chem.* **35**, 1197 (1997).
16. S. J. Gregg, and K. S. W. Sing: *Adsorption, Surface Area and Porosity, 2nd edn*, Academic Press, New York, pp. 41–54 (1982).
17. G. F. Cerofolini and L. Meda: *J. Colloid Interface Sci.* **202**, 104 (1998).
18. A. L. Spek: *PLATON99, A Multipurpose Crystallographic Tool*, Utrecht University, Utrecht, The Netherlands (1999).
19. T. Kawai and K. Tsutsumi: *Colloid Polym. Sci.* **273**, 787–792 (1995).